*J. Fluid Mech.* (1974), *vol.* 66, *part* 4, *pp.* 739–752
*Printed in Great Britain*



# Interferometric study of two-dimensional Bénard convection cells

By R. FARHADIEH AND R. S. TANKIN

Gas Dynamics Laboratory, Northwestern University,
Evanston, Illinois 60201

(Received 11 June 1973 and in revised form 5 February 1974)

A Mach–Zehnder interferometer was used to study two-dimensional Bénard convection cells. The experiments were performed with distilled water and sea water in the region where density is a linear function of temperature. Two-dimensional convection rolls were formed with Rayleigh numbers as great as 23400. Reversal in the temperature profile was obtained for $R/R_c \geqslant 3{\cdot}8$, and an overshoot of about 6 % was observed at $R/R_c = 9{\cdot}2$ and 13·8. This agrees with the values predicted theoretically by Veronis (1966) for stress-free boundaries and Royal (1969) for rigid boundaries. This disagrees with the experimental results of Gille (1967), who reports an overshoot of only $1\frac{1}{2}$ % at $R/R_c = 16$. Many of the other results agree with those of other experimenters, such as the relation between the cell height-to-width ratio and Rayleigh number, the relation between the Nusselt number and Rayleigh number, and the value of the critical Rayleigh number.

## 1. Introduction

Thermal instability across a horizontal layer of fluid confined between two rigid boundaries is the topic of these experiments. This study is confined to a temperature region where the density of the test fluid is a linear function of temperature. Although freezing is not the subject of this study, it is our eventual goal. The freezing experiments will concentrate on the interaction between the convection currents in the fluid and the solid–liquid interface. For freezing, sea water and distilled water will be used as the test fluids since their behaviour is significantly different: one has a positive coefficient of thermal expansion near freezing, whereas for the other it is negative. In the present study, convection currents in the liquid are studied in detail. The reasons for using sea water in these experiments are to determine the corrosion resistance of the apparatus and the accuracy of temperatures obtained from an interferogram (the relation between the temperature and index of refraction). The sea water used was obtained from the Shedd Aquarium in Chicago and its salinity was regulated by adding either NaCl or distilled water.

There are many theoretical studies (Rayleigh 1916; Pellew & Southwell 1940; Chandrasekhar 1961, etc.) and experimental studies (Bénard 1901; Schmidt & Milverton 1935; Silveston 1958, etc.) which verify that, when a

horizontal layer of fluid is subjected to an adverse temperature gradient, it becomes unstable to infinitesimal disturbances if a critical Rayleigh number is exceeded. Schmidt & Milverton (1935), Silveston (1958) and others deduced the existence of the instability experimentally by measuring the Nusselt number over a wide range of Rayleigh numbers. In 1966, Veronis obtained a numerical solution for the steady-state problems involving large amplitude convection. This study was restricted to the case of stress-free boundaries. The computed temperature profiles show a temperature reversal in the central portion of the fluid when the Rayleigh number exceeds $4R_c$. The temperature overshoots the mean temperature by 6% of the total temperature drop across the layer for large Rayleigh numbers. Veronis' calculations show that the temperature overshoot is essentially independent of Prandtl number. Royal (1969) found a numerical solution for large amplitude convection with rigid boundaries. His results show a temperature reversal of about 7% at large Rayleigh numbers. Attempts have been made to measure temperature profiles with probes, but these results did not reveal a temperature reversal. Gille (1967) performed experiments on a layer of air in which a Michelson interferometer was used as the temperature sensing device. He did not detect a temperature reversal at $R/R_c = 3{\cdot}81$ but did at $R/R_c = 16$. However, the temperature reversal he detected was only $1\frac{1}{2}$%, which did not agree with theory.

Schneck & Veronis (1967) made calculations of the Nusselt number *vs.* the Rayleigh number. In these calculations, they assumed the cell height-to-width ratio to be 1·0 and their computed Nusselt numbers were higher than the experimental results of Rossby (1969) and others. This discrepancy between theory and experiment increases with increasing Rayleigh number. Willis, Deardorff & Sommerville (1972) measured the dependence of the cell height-to-width ratio on the Rayleigh number and found that this ratio decreases with increasing Rayleigh number. Busse (1967) investigated the stability of two-dimensional rolls at large Rayleigh numbers and found that these rolls become unstable when the Rayleigh number exceeds 22600.

The main purpose of this study is to establish the presence of a temperature reversal and determine the magnitude of its overshoot at large Rayleigh numbers. In addition, many of the results are compared with the findings of other investigators, such as the cell height-to-width ratio as a function of Rayleigh number, the existence of an upper limit on the Rayleigh number for two-dimensional rolls, the Nusselt number as a function of Rayleigh number, and the critical Rayleigh number.

## 2. Experimental apparatus and procedure

Temperature probes give the temperature at isolated points within the test section. However, if the temperature variation is two-dimensional and aligned along the optical axis, an interferogram will yield the temperature at all points in the test section. This is achieved without disturbing the flow. Thus a Mach–Zehnder interferometer, which is an ideal instrument when the fluids are transparent to visible light, was employed.

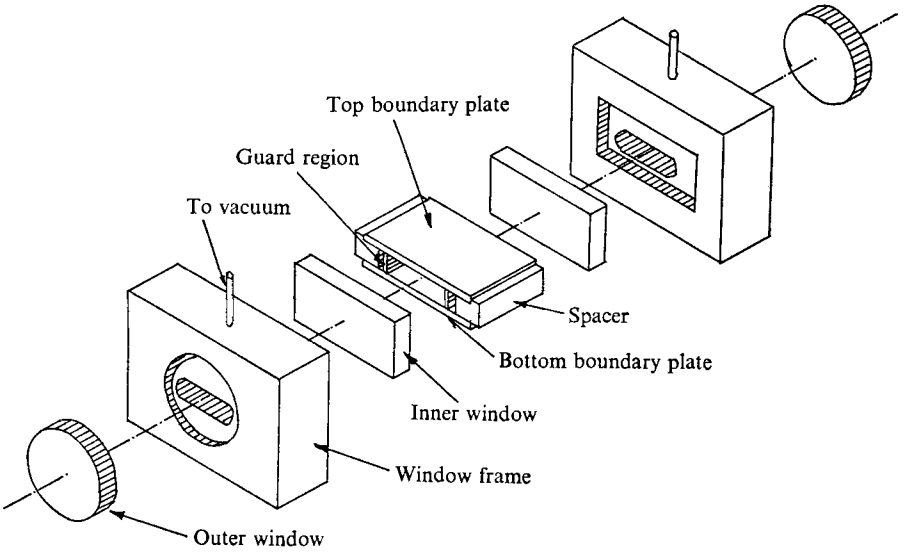


FIGURE 1. Schematic drawing of test section.

The optics throughout the system, beam splitters, front-surfaced mirrors, windows of the test section, etc., are flat to within $\frac{1}{10}$ wavelength. A neon–helium laser is used as a light source for the interferometer. The entire system, interferometer, test section and focusing mirrors, is mounted on a vibration-isolated table. The test section is rectangular, having a cross-section of 20·3 × 7·6 cm and a depth of either 0·635 cm or 0·95 cm. Davis (1967), Segel (1969) and Davies-Jones (1971) obtained theoretical results indicating that when Bénard rolls develop in a rectangular test section they are oriented with their axes parallel to the short side of the test section. This result was experimentally verified by Stork & Müller (1972). Thus, in our experimental set-up, the test section is oriented so that the short side (7·62 cm) is along the optical axis.

The top and bottom plates of the test section are made of stainless steel, 1·27 cm thick and ground flat (to $\pm$ 0·0025 cm). This material was used because it resists corrosion by sea water. Thermoelectric modules are mounted on the exterior of these plates, allowing one to maintain preselected temperatures by carefully controlling the power input to the thermoelectric modules. The depth of the test section is determined by the height of Plexiglas spacers which serve as the ends of the test section. These spacers have troughs machined in them to eliminate any pressure changes in the test section due to thermal expansion and contraction of the liquid. This is of particular importance when freezing experiments are performed. The front and back of the test section, through which the laser light passes, are windows. Each of these windows is made of optical flats with a vacuum between them (thermopane fashion). A schematic drawing of the test section is shown in figure 1.

Teflon-coated thermistors were inserted in holes in the top and bottom plates which were 0·50 cm from the surface of the test fluid. During the experiment,

their outputs were recorded on a two-channel strip-chart recorder. Before and after each experiment, the thermistors were calibrated, and an accuracy of about 0·10 °C was obtained. Copper–constantan thermocouples were used to measure the temperature difference (heat flux) across the top and bottom plates. The outputs from the thermocouples were amplified and recorded on a strip-chart recorder. An accuracy of 0·01 °C or better was obtained with these thermocouples.

To ensure uniform heating (or cooling) of the top and bottom plates, the following experimental arrangement was used. The thermoelectric modules were soldered to a brass plate through which cooling water from a constant-temperature circulator flowed. The other surfaces of the thermoelectric modules were clamped to a 0·95 cm thick copper plate (both surfaces ground flat). This copper plate was then clamped to the exterior of the stainless-steel plate (the top or bottom plate of the test section). Between all of the clamped surfaces, a heat-sink compound (Dow Corning 340) was applied. This arrangement gave very uniform heating of the top and bottom plates as can be seen from the straight parallel fringes (isotherms) in the vicinity of the plate (see figure 3*a*, plate 1). The temperature difference between each pair of fringes is about 0·1 °C.

Most of the interferograms were recorded with a 35 mm camera having a shutter speed of $\frac{1}{250}$ s. A parabolic front-surfaced mirror was used to focus the centre-plane of the test section on the film. No lenses were used in the system except for the one used in the spatial filter assembly of the laser light source. Interferograms were taken half an hour after each incremental increase in the input current to the thermoelectric modules. This time was allowed to ensure steady-state conditions in the test fluid.

The test fluids used in these experiments were boiled to remove dissolved air, thus reducing the chance of bubbles appearing in the text section. The salinity of the sea water was checked before each experiment and the test section was refilled with new fluid after each sequence of experiments. With the optics in close alignment, the test section in place and the fluid at a uniform temperature, the final adjustments to the interferometer for infinite fringe spacing were made. When a temperature variation occurs in the test section, each fringe is a contour line of constant phase shift of the light. If the optical path length (width of test section) and the wavelength of the light are known, the change ($7{\cdot}37 \times 10^{-6}$) in the index of refraction between each fringe can be computed. Having the index of refraction as a function of temperature (from Tilton & Taylor's (1938) data for distilled water, from calibration or use of Montgomery's (1955) data for sea water) and measuring the temperature at one point in the test section, one can determine the temperature at all points in the test section. Each fringe represents an isotherm.

Steady-state experiments were performed as follows. The test section was filled with water and allowed to sit for several hours to ensure uniform conditions; then infinite-fringe adjustments were made on the interferometer. Cooling water from the constant-temperature circulator was pumped through the external plates attached to the thermoelectric modules. Once equilibrium was reached (about 16 °C) in the test section, the infinite-fringe condition returned. The system was maintained at this condition for about 2 h to ensure equilibrium

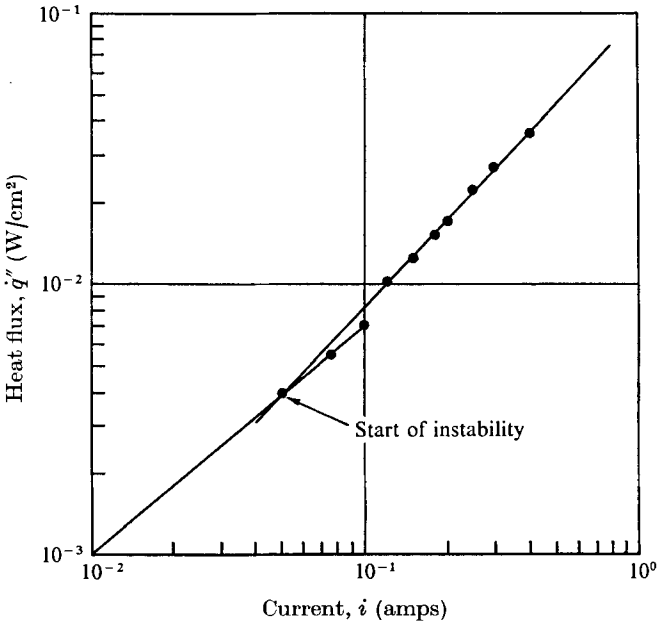


FIGURE 2. Electric current (in amps) supplied to thermoelectric modules *vs.* heat flux to the test section.

before the experiment was started. Then heat was applied to the bottom plate while an equal amount was extracted from the top plate. This constant heat flux was maintained for at least half an hour to allow the system to reach a steady state. This time exceeds the thermal diffusion times for water layers 0·635 cm and 0·952 cm deep (approximately 5 min and 10 min respectively). The electric current supplied to the thermoelectric modules was continuously monitored with a digital voltmeter. A slow increase in the heat flux was extremely important for the initial formation of two-dimensional convection rolls. The temperatures of the plates were initially changed in increments of 0·05 °C or less. It should be mentioned that the mean temperature of the water in the test section varied only negligibly since the heat fluxes through the top and bottom plates were the same. Once the convection rolls were well established (see, for example, figure 3*e*, plate 1), the incremental change in the temperatures of the top and bottom plates was no longer critical. Figure 2 shows the relation between the current input (in amps) to the thermoelectric modules and the heat flux to the fluid (in W/cm$^2$).

To indicate the nature of the convection pattern, a separate experiment was performed. The top plate was removed, a convection pattern established and a dye particle (DuPont Victoria Green) dropped into the test section. This dye particle sank to the bottom and dissolved, yielding streaklines, which were green and clearly visible on the interferograms.

| | Salinity (‰) | Kinematic viscosity $\nu$ ($cm^2 s^{-1} \times 10^3$) | Thermal diffusivity $\kappa$ ($cm^2 s^{-1} \times 10^3$) | Thermal conductivity $K$ ($W cm^{-2} °C \times 10^3$) | Coefficient of volume expansion $\alpha$ ($°C^{-1} \times 10^4$) |
|---|---|---|---|---|---|
| Distilled water | 0 | 1·1 | 1·43 | 5·8 | 1·43 |
| Sea water | 35 | 1·049 | 1·49 | 5·8 | 2·27 |
| Sea water | 40 | 1·049 | 1·49 | 5·8 | 2·35 |

TABLE 1. Physical properties of test fluid at about 16 °C

## 3. Experimental results and discussion

Table 1 gives some of the pertinent properties of the test fluids in the neighbourhood of 16 °C. For these fluids, the variations in thermal diffusivity and kinematic viscosity are approximately 0·03 % and 0·3 % per degree respectively. Since the temperature range in these experiments is less than 2 °C, these quantities are assumed to be constant. The coefficient of volume expansion is of the order of $10^{-4}$. These conditions satisfy the requirements for the Boussinesq approximation.

The Rayleigh number, which determines the strength of the convection cells, is defined as

$$R = g\alpha\Delta T d^3/\nu\kappa,$$

where $g$ is the acceleration due to gravity (in cm/s$^2$), $\alpha$ is the coefficient of volume expansion (in °C$^{-1}$), $d$ is the depth of the fluid layer (in cm), $\Delta T$ is the temperature difference between the top and bottom plates (in °C), $\nu$ is the kinematic viscosity (in cm$^2$/s) and $\kappa$ is the thermal diffusivity (in cm$^2$/s). At the onset of instability $R = R_c$. Figure 3(*a*) (plate 1) is an interferogram taken before a temperature variation is imposed between the top and bottom plates; the temperature of the fluid in the test section is uniform (16 °C). A uniform temperature in the test section is assured since the infinite-fringe condition appears. Figure 3(*b*) (plate 1) shows the appearance of isotherms when a temperature variation is imposed on the test fluid. These isotherms are equally spaced and parallel to the boundary plates; thus there is no convection in the test section, i.e. the critical Rayleigh number has not been reached. The temperature difference between neighbouring fringes is about 0·1 °C. Therefore, in figure 3(*b*), the temperature difference between the top and bottom plates is 0·55 °C, which checks with the thermistor readings. When the critical Rayleigh number is reached, the fringes are no longer straight, having a small amplitude deviation which is sinusoidal in appearance. This is shown in figure 3(*c*) (plate 1). The isotherm spacing near the top and bottom plates is less than the spacing in the central region of the test section. This is expected, because near the boundaries heat transfer is by conduction; whereas, in the central region of the test section, heat transfer is by convection.

The experimental values of the critical Rayleigh number are listed in table 2. These values were obtained by examining interferograms such as figure 3(*c*). Another method of determining the critical Rayleigh number, used by previous

| | Depth $d$ (cm) | Rayleigh number $R$ | Temperature difference $\Delta T$ (°C) | $R/R_c$ | Heat flux $\dot{q}''$ (W cm$^{-2}$ $\times 10^2$) | Nusselt number $Nu$ |
|---|---|---|---|---|---|---|
| Distilled water | 0·635 | 1700 ± 20† | 0·74 | 1·00 | 0·4 | 1·0 |
| | 0·635 | 2 410 | 0·95 | 1·42 | 1·25 | 1·45 |
| | 0·635 | 3 740 | 1·48 | 2·2 | 2·45 | 1·82 |
| | 0·635 | 4 600 | 1·78 | 2·7 | 3·2 | 1·96 |
| | 0·635 | 6 450 | 2·56 | 3·8 | 5·1 | 2·18 |
| Sea water of salinity 35 ‰ | 0·635 | 1700 ± 20† | 0·57 | 1·00 | — | — |
| | 0·635 | 2 720 | 0·8 | 1·6 | 1·1 | 1·45 |
| | 0·635 | 3 540 | 1·05 | 2·08 | 1·75 | 1·8 |
| | 0·635 | 4 750 | 1·41 | 2·8 | 2·45 | 1·9 |
| | 0·9525 | 23 500 | 1·87 | 13·8 | 3·15 | 2·76 |
| Sea water of salinity 40 ‰ | 0·635 | 1700 ± 30† | 0·55 | 1·00 | — | — |
| | 0·635 | 3 050 | 0·82 | 1·8 | 1·1 | 1·46 |
| | 0·635 | 3 900 | 1·02 | 2·3 | 1·55 | 1·66 |
| | 0·635 | 5 275 | 1·4 | 3·1 | 2·45 | 1·91 |
| | 0·635 | 7 650 | 1·99 | 4·5 | 3·65 | 2·00 |
| | 0·9525 | 15 600 | 1·18 | 9·2 | 1·75 | 2·45 |

† $R = R_c$

TABLE 2. Summary of experimental results

investigators, is to plot the Nusselt number *vs.* the Rayleigh number. A break in the slope of the curve gives the critical Rayleigh number. This is shown in figure 2 and the result agrees with the value obtained from the interferogram. As the heat flux is increased, the amplitude of the fringe deviation from straight fringes increases and the fringe pattern deviates from being sinusoidal (figures 3–5, plates 1–3). In fact, there is a reversal in temperature gradient on the interferograms (figures 3*g*, 4*d*, 5*d*, *e*).

To demonstrate the two-dimensionality of the flow and to indicate the convection pattern, a dye particle was introduced into the test section. This dye particle settled in the trough of the isotherm pattern. A streakline (taken about 2 s later) shows the dye moving to the right and left along the bottom (figure 6*a*). A sequence of pictures showing the circulation pattern is shown in figure 6 (plate 4). Figure 6(*f*) shows the streaklines schematically. The convection pattern can be deduced from the interferograms as follows: where the isotherms (fringes) are concave upwards (trough) cold water (more dense) moves downwards; it then reaches the bottom, moves laterally and becomes warmer; finally, it moves upwards where the isotherms (fringes) are concave downwards (peak). Thus the circulation pattern is a closed cell: cold water moves downwards and is heated as it moves horizontally near the bottom plate; warm water moves upwards and is cooled as it moves horizontally near the top plate.

Figure 7 (plate 5), an enlargement of figure 4(*c*), was used to obtain the non-dimensional temperature profiles shown in figure 8. The 'upflow' (curve *c*) and 'downflow' (curve *a*) were obtained by counting fringes along the lines *AA* and *BB* respectively in figure 7. These lines approximately define the cell boundaries. The slope of the 'upflow' curve (*c*) near the top plate is identical with the slope of

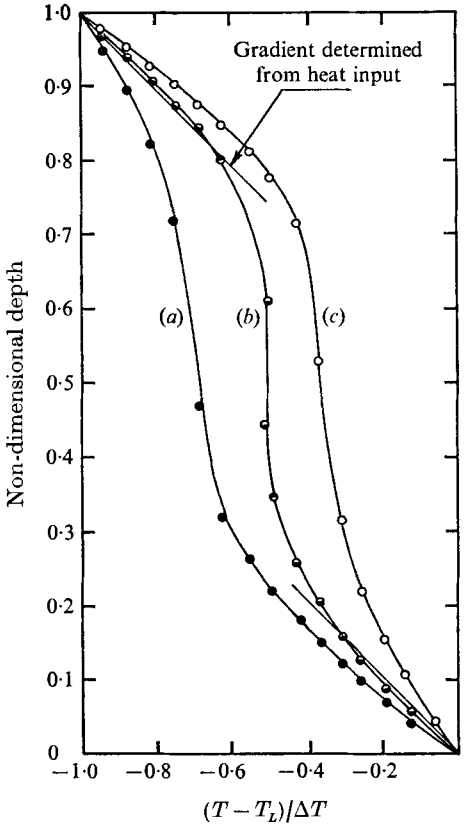


FIGURE 8. Temperature profiles obtained from interferogram shown in figure 7. $Pr = 6{\cdot}8$; $R/R_c = 2{\cdot}8$. (*a*) Downflow. (*b*) Horizontal average over half-cell. (*c*) Upflow.

the 'downflow' curve (*a*) near the bottom plate. Identical relations apply to other corresponding portions of the curves. Since the fluid convection is related to the isotherm pattern, a symmetry in isotherm patterns implies a symmetry in the convection.

The horizontally averaged temperature profile, curve (*b*) in figure 8, was obtained by dividing the distance between $AA$ and $BB$ in figure 7 into ten equal intervals. The temperature measurements at each of these intervals (at a preselected vertical position) were averaged. This procedure was used to obtain the temperature profiles in figures 9(*a*), (*b*) and (*c*) from the interferograms shown in figures 3, 4 and 5. The horizontally averaged temperature profiles are antisymmetric with respect to the point $(T-T_L)/\Delta T = 0{\cdot}5$, $x/d = 0{\cdot}5$. The straight lines near the boundaries ($x/d = 0$ and $x/d = 1$) in figure 8 are computed non-dimensional temperature gradients that were obtained from the conduction measurements (thermocouples) across the stainless-steel plates. It is seen that the computed temperature gradients at the boundaries are in close agreement with the horizontally averaged values (curve *b*). Figure 10 shows the results from three experiments with essentially the same Rayleigh numbers. This indicates the reproducibility of the data. The temperature profiles in figure 9 span a wide

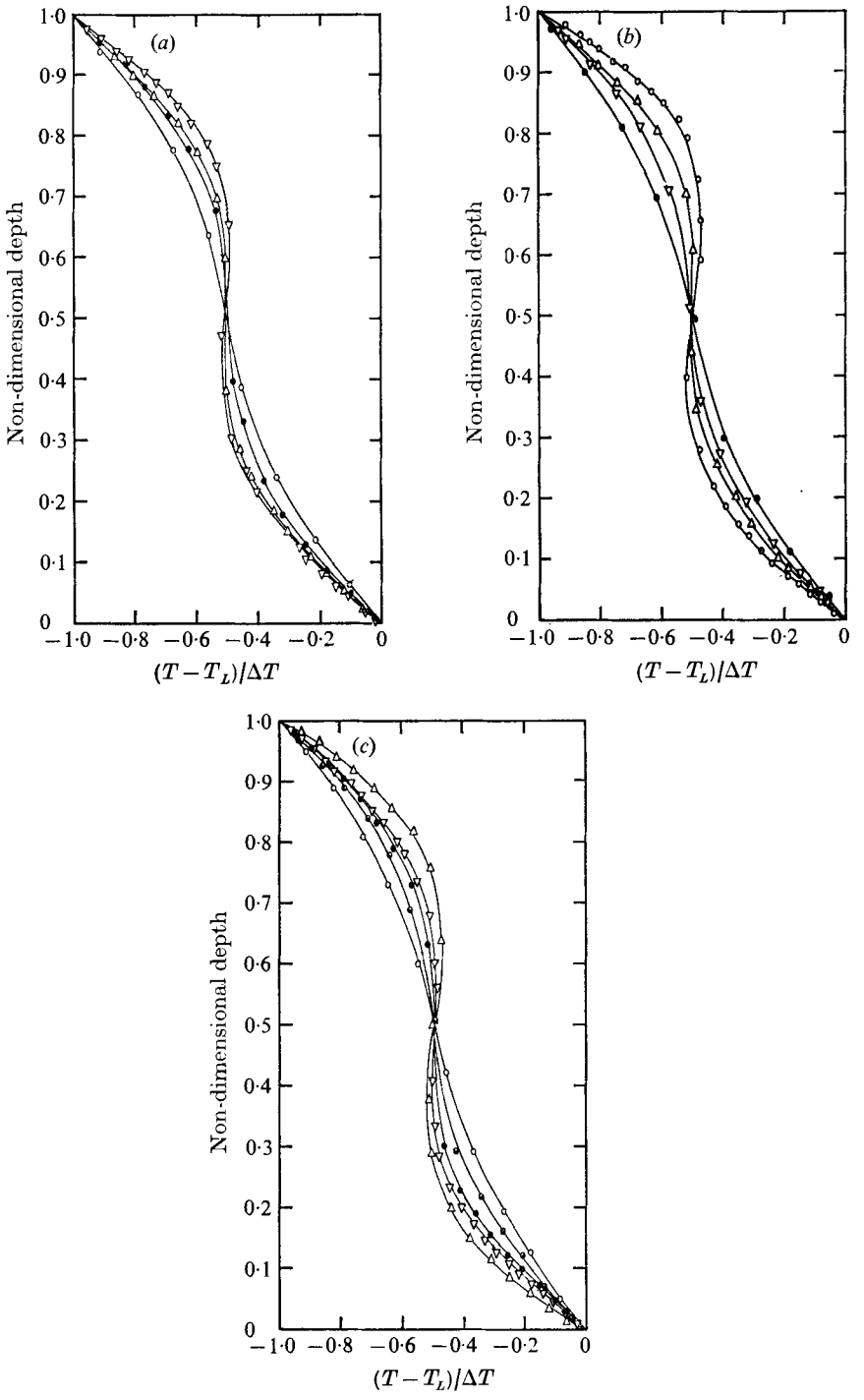


FIGURE 9. Horizontally averaged temperature profiles at various Rayleigh numbers. (*a*) Distilled water. (*b*) Sea water of salinity 35‰. (*c*) Sea water of salinity 40‰.

| | ○ | ● | △ | ▽ | ◓ |
|---|---|---|---|---|---|
| (*a*) $R/R_c$ | 1·42 | 2·2 | 2·7 | 3·8 | |
| (*b*) $R/R_c$ | 13·8 | 1·6 | 2·8 | 2·08 | |
| (*c*) $R/R_c$ | 1·8 | 3·1 | 9·2 | 4·5 | 2·3 |

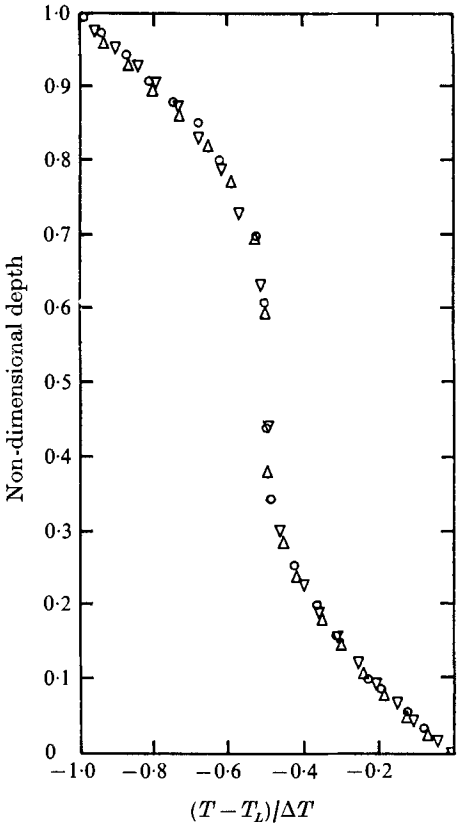


FIGURE 10. Horizontally averaged temperature profiles at approximately the same Rayleigh number. This indicates reproducibility of data. $Pr = 6{\cdot}8$. △, $R/R_c = 2{\cdot}7$; ○, $R/R_c = 2{\cdot}8$; ▽, $R/R_c = 3{\cdot}1$.

range of Rayleigh numbers. In all cases, the slopes of these curves are negative near the boundaries, where conduction is predominant. The slopes, near the boundaries, become more negative with increasing Rayleigh number. In the central region of the test section, where convection is predominant, the slope remains negative at low Rayleigh numbers ($R/R_c < 3{\cdot}8$), is infinite at $R/R_c \approx 3{\cdot}8$ and is positive for $R/R_c > 3{\cdot}8$. This positive slope in the central region of the test section is known as temperature reversal. As the strength of the convection increases (increasing Rayleigh number), the reversal in the temperature profile becomes more pronounced. At large Rayleigh numbers, the temperature overshoots the mean temperature of the fluid by about 6 % of the total temperature drop across the fluid layer. From the temperature profiles in figure 9 one can see that the convection layer fills a larger portion of the test section as the Rayleigh number increases.

Veronis (1966) computed temperature profiles for stress-free conditions at the boundaries. These computations show a small reversal at $R/R_c = 4{\cdot}0$, an overshoot in the temperature profile of about 6 % at high Rayleigh numbers and a broadening of the convective layer with increasing Rayleigh number. More

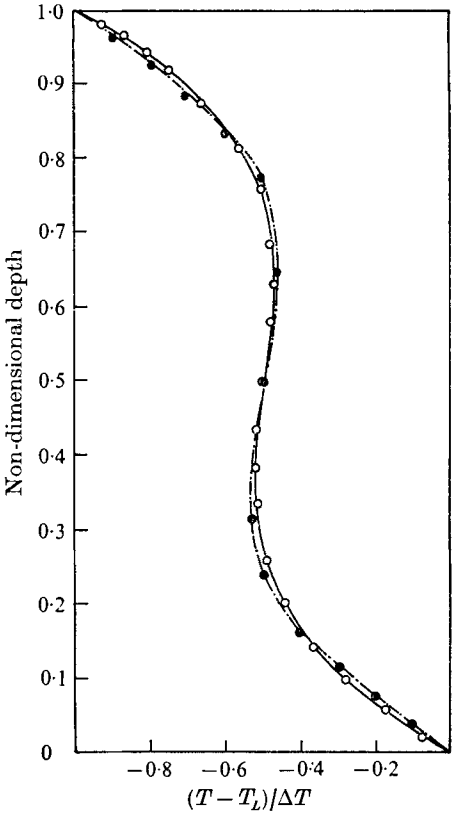


FIGURE 12. Comparison between experimental and computed temperature profiles. ○, this study, $R = 15\,640$, $Pr = 6{\cdot}8$; ●, theoretical study of Royal, $R = 10\,000$, $Pr = 0{\cdot}7$.

recent computations were carried out by Royal (1969). The computations were made for rigid boundaries at a Rayleigh number of 10 000 and a Prandtl number of 0·7. In figure 11 (plate 6) his computed isotherms are superimposed on an interferogram where the Rayleigh number is 6460. One difficulty in comparing the theoretical and experimental values is that the theoretical values were computed under the assumption that the cell height-to-width ratio is 1; this was not found to be the case experimentally. Experimentally, the cell height-to-width ratio decreases with increasing Rayleigh number. One cannot simply distort the horizontal-to-vertical scale ratio in the computed results in order to compare experiment and theory. However, it can be seen that there is qualitative agreement between theory and experiment. To achieve a better comparison, a vertical temperature profile was taken midway between the peak and trough of an experimental test and compared with Royal's computed results. This comparison is shown in figure 12, and agreement between theory and experiment is excellent. The only other experiments of which the authors are aware that show a temperature reversal are those of Gille (1967). However, his results indicate a reversal of at most $1\frac{1}{2}\%$. There are two points that should be mentioned with regard to Gille's results. First, his experiment was conducted with air as the test fluid;

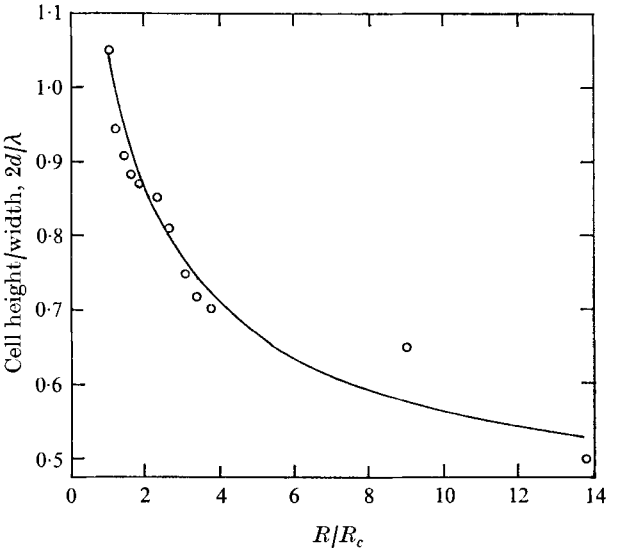


FIGURE 13. Plot showing cell height-to-width ratio *vs.* Rayleigh number. ○, this study; ——, Willis *et al.*

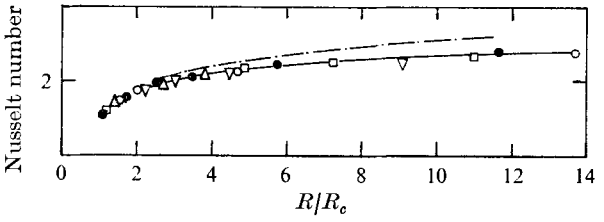


FIGURE 14. Comparison of computed and experimental Nusselt numbers. $Pr = 6{\cdot}8$. Experimental results: △, ○, ▽, this study; □, Silveston; ●, Rossby. —·—, theory, Schneck & Veronis.

whereas the experiments carried out in this study were with water. Although the Prandtl number for air is much smaller than that for water (0·7 compared with 6·8), Veronis obtained essentially the same temperature reversal for Prandtl numbers equal to 6·8 and 0·025. In addition, Royal's computations were made for a Prandtl number equal to 0·7. Thus, one would expect the temperature reversal for water and air to be about the same (about 6%). Second, Gille's result was obtained at a Rayleigh number of 27500. Busse (1967) and Busse & Whitehead (1971) report that, at Rayleigh numbers above 23000, rolls are unstable at all wavenumbers and are replaced by a three-dimensional instability. Thus, Gille may not have observed two-dimensional rolls in his experiment.

Figure 13 shows the relationship between the Rayleigh number and the cell height-to-width ratio $2d/\lambda$. At the onset of instability this ratio is about 1·05 (see figure 3*c*), but as the Rayleigh number increases it decreases to 0·5 for $R = 13{\cdot}8\,R_c$. These results agree with the experimental values of Willis *et al.* (1972). The measurements in figure 13 were obtained directly from the interferograms in figures 3–5.

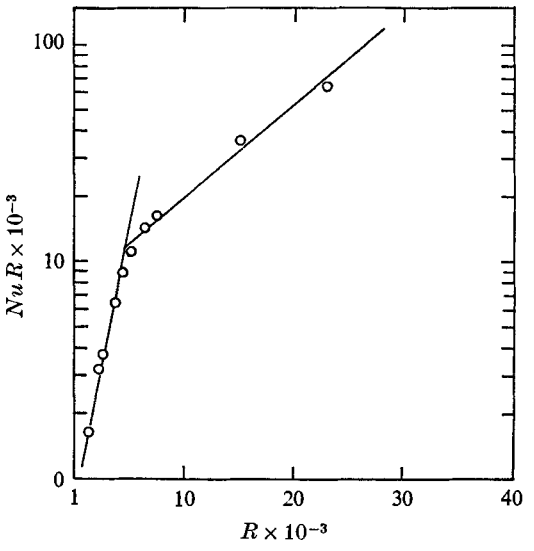


FIGURE 15. A semi-logarithmic plot of the experimental data shown in figure 14. This indicates a change in the relation between the Nusselt number and Rayleigh number.

The Nusselt number was calculated from the relationship

$$Nu = \dot{q}''d/K\Delta T,$$

where $\dot{q}''$ is the heat flux measured across the top (or bottom) plate and $K$ is the thermometric conductivity of the fluid layer. A plot of the Nusselt number as a function of Rayleigh number is shown in figure 14. As can be seen, these experimental results agree with those of other experimentalists. Certain characteristics of the relationship between the Nusselt number and Rayleigh number may be worth mentioning. There is a relatively strong increase in the Nusselt number with Rayleigh number in the range $1 < R/R_c < 3$; the increase in the Nusselt number becomes more gradual for $R/R_c > 4$. In the range $1 < R/R_c < 3$ convection is established, but there is no reversal in temperature: an increase in convection strongly affects the heat transfer. However, when $R/R_c > 4$ convection increases with Rayleigh number; but the heat transfer increases relatively slowly with increasing Rayleigh number (see figure 15). A physical explanation is as follows: at high Rayleigh numbers (above $4R_c$) the cold water that plunges downwards does not have sufficient time to be warmed by molecular heat conduction and therefore spreads out near the bottom without absorbing much heat from the bottom plate; likewise, the warm water which rapidly rises spreads out near the top without transferring much of its heat to the top plate. Thus, although the convection increases significantly, the heat flux only increases slowly. This is also an explanation for the reversal in temperature that is seen on the interferograms (figures 4*d*, 5*d*, *e*).

The Nusselt number *vs.* Rayleigh number relation found in this study agrees with the experimental values of Silveston (1958) and Rossby (1969). However, the experimental results yield Nusselt numbers that lie below those predicted

theoretically by Schneck & Veronis (1967) and Busse (1967). This discrepancy between theory and experiment increases with increasing Rayleigh number. The heat transfer (Nusselt number) is dependent on the cell height-to-width ratio. The theoretically computed Nusselt number is based on a cell height-to-width ratio equal to one; whereas, the experimental results show this ratio to be less than one, decreasing with increasing Rayleigh number (see figure 13). If the experimental cell height-to-width ratio had been used in computing the Nusselt number, the computed Nusselt number would have been less. This is an explanation given by Willis *et al.*, with which we agree.

## 4. Conclusions

An interferogram gives a complete picture of the isotherm pattern as well as a quantitative temperature distribution throughout the test section. This study verifies the theoretical result that a temperature overshoot of about 6 % occurs at high Rayleigh numbers. This temperature reversal first appears at $R/R_c = 3{\cdot}8$.

In addition, the results of this interferometric study on two-dimensional rolls are consistent with many of the results reported by other investigators: for example, (i) the critical Rayleigh number is $1700 \pm 30$; (ii) the height-to-width ratio decreases with Rayleigh number; (iii) two-dimensional rolls are stable at Rayleigh numbers below 23400.

The Office of Naval Research under contract N00014-67-A-0356-0021 provided financial support for this study. The authors thank J. Witting and A. Hanson for many helpful suggestions.

REFERENCES

BÉNARD, H. 1901 *Ann. Chim. Phys.* **23**, 62–144.

BUSSE, F. H. 1967 *J. Math. & Phys.* **46**, 140–150.

BUSSE, F. H. & WHITEHEAD, J. A. 1971 *J. Fluid Mech.* **47**, 305–320.

CHANDRASEKHAR, S. 1961 *Hydrodynamic and Hydromagnetic Stability*. Clarendon Press.

DAVIES-JONES, R. P. 1971 *J. Fluid Mech.* **44**, 695–704.

DAVIS, S. 1967 *J. Fluid Mech.* **30**, 465–478.

GILLE, J. 1967 *J. Fluid Mech.* **30**, 371–384.

MONTGOMERY, R. B. 1955 *American Institute of Physics Handbook*, 2nd ed., pp. 2–123.

PELLEW, A. & SOUTHWELL, R. V. 1940 *Proc. Roy. Soc.* A **176**, 312–343.

RAYLEIGH, LORD 1916 *Phil. Mag.* **32**, 529–546.

ROSSBY, H. T. 1969 *J. Fluid Mech.* **36**, 309–335.

ROYAL, J. W. 1969 Dissertation Boston University.

SCHMIDT, R. J. & MILVERTON, S. W. 1935 *Proc. Roy. Soc.* A **152**, 586–594.

SCHNECK, P. & VERONIS, G. 1967 *Phys. Fluids*, **10**, 927–930.

SEGEL, L. A. 1969 *J. Fluid Mech.* **38**, 203–224.

SILVESTON, P. L. 1958 *Forsch. Ing. Wes.* **24**, 29–32, 59–69.

STORK, K. & MÜLLER, U. 1972 *J. Fluid Mech.* **54**, 599–611.

TILTON, L. W. & TAYLOR, J. K. 1938 *J. Res. Nat. Bur. Stand.* **20**, 419–465.

VERONIS, G. 1966 *J. Fluid Mech.* **26**, 49–68.

WILLIS, G. E., DEARDORFF, J. W. & SOMERVILLE, R. C. J. 1972 *J. Fluid Mech.* **54**, 351–367.

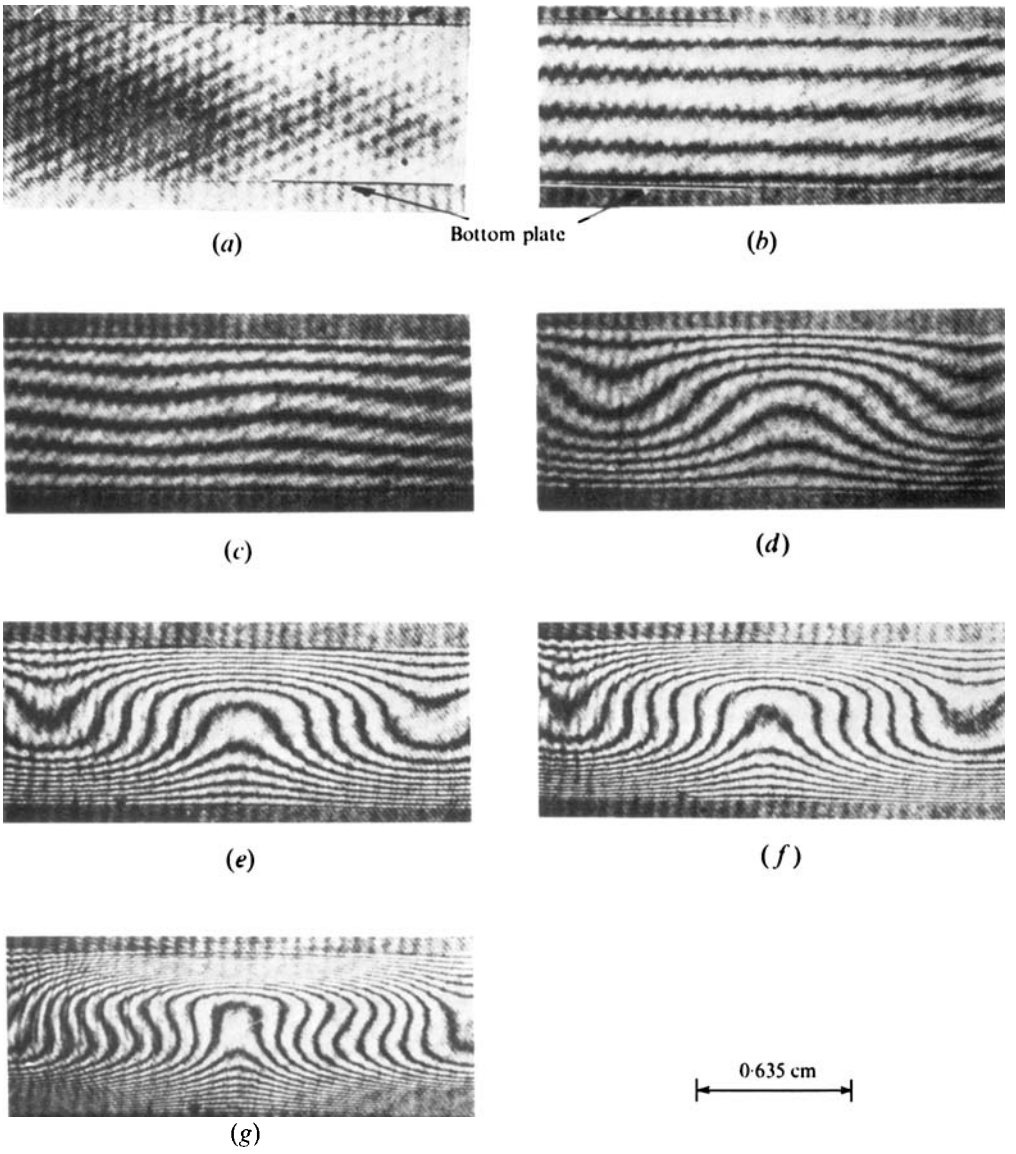


FIGURE 3. Sequence of interferograms showing isotherms in test section. The fluid is distilled water; $Pr = 6{\cdot}8$. (*c*) $R = R_c = 1700 \pm 20$. (*d*) $R/R_c = 1{\cdot}42$. (*e*) $R/R_c = 2{\cdot}2$. (*f*) $R/R_c = 2{\cdot}7$. (*g*) $R/R_c = 3{\cdot}8$.

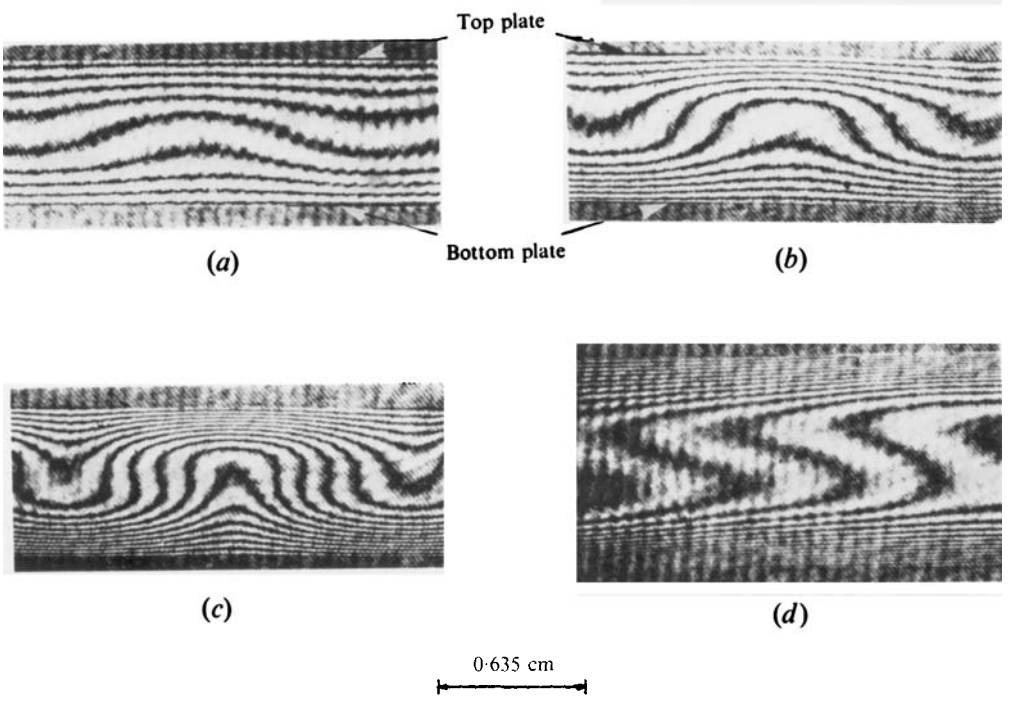


FIGURE 4. Sequence of interferograms showing isotherms in test section. The fluid is sea water of salinity (35‰). (*a*) $R/R_c = 1{\cdot}6$. (*b*) $R/R_c = 2{\cdot}08$. (*c*) $R/R_c = 2{\cdot}8$. (*d*) $R/R_c = 13{\cdot}8$.

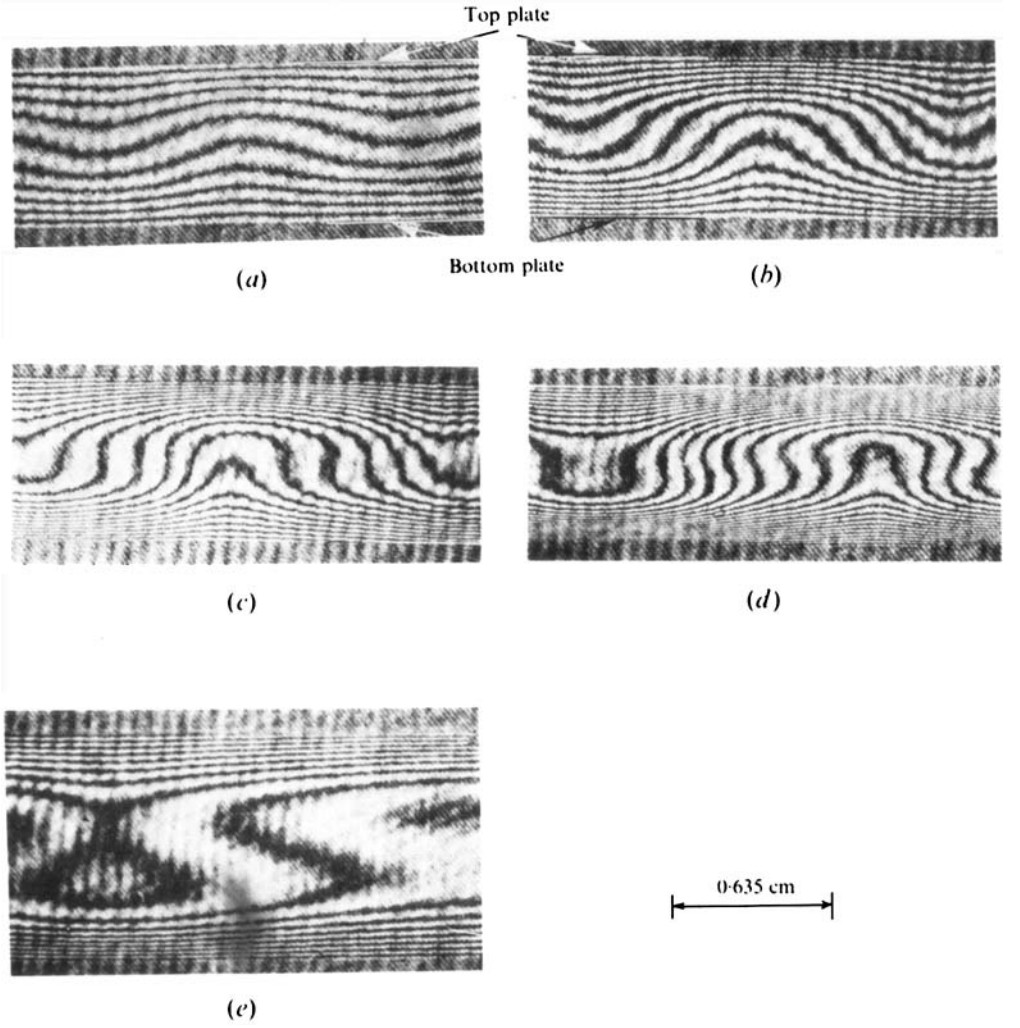


FIGURE 5. Sequence of interferograms showing isotherms in test section. The fluid is sea water of salinity (40‰). (*a*) $R/R_c = 1{\cdot}8$. (*b*) $R/R_c = 2{\cdot}3$. (*c*) $R/R_c = 3{\cdot}1$. (*d*) $R/R_c = 4{\cdot}5$. (*e*) $R/R_c = 9{\cdot}2$.

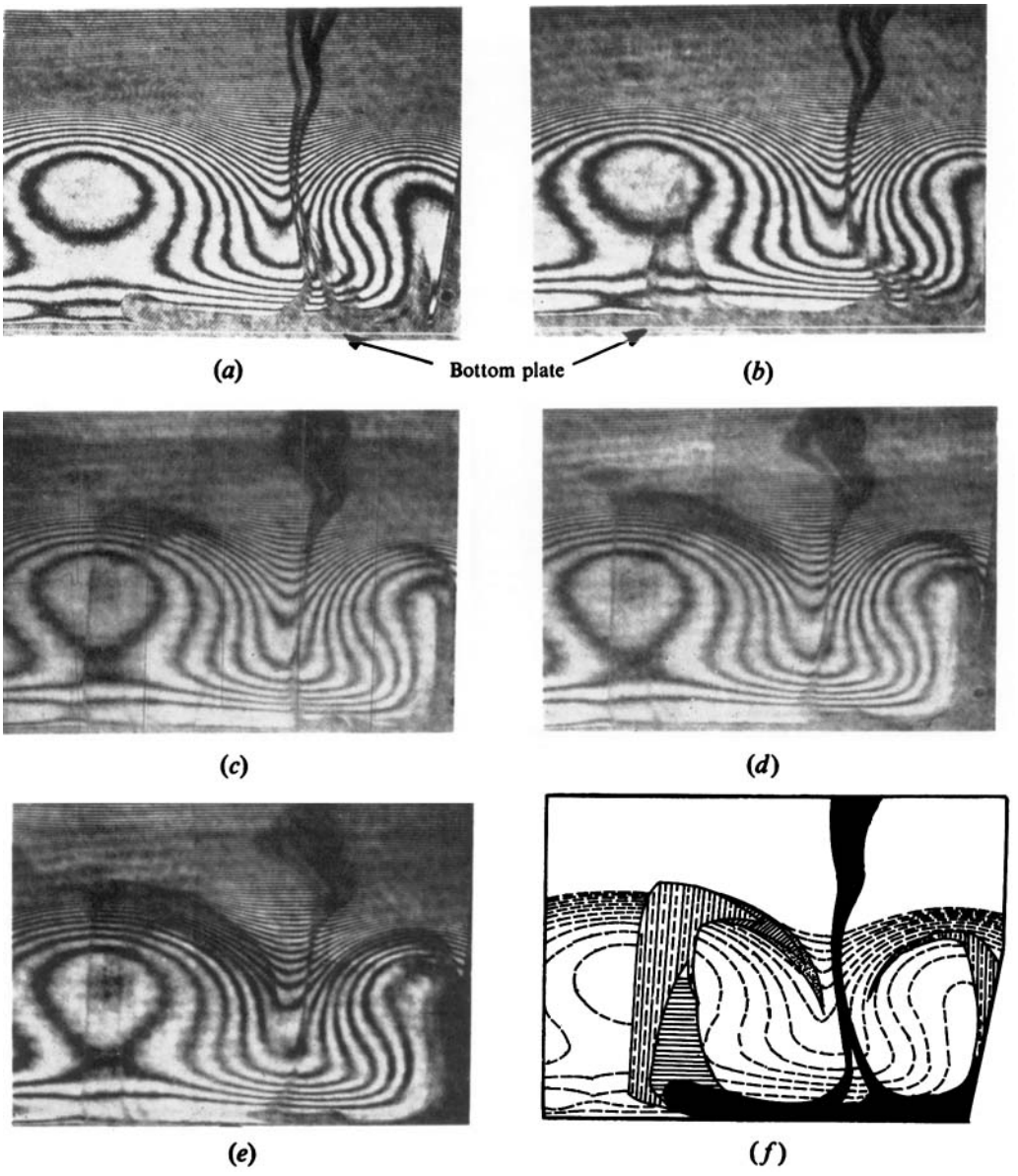


FIGURE 6. Sequence of interferograms showing streaklines from dye particle. Dye filaments traced in (*f*): ■, from (*a*); ▤, from (*b*); ▥, from (*c*), ▨, from (*d*); ▦, from (*e*).

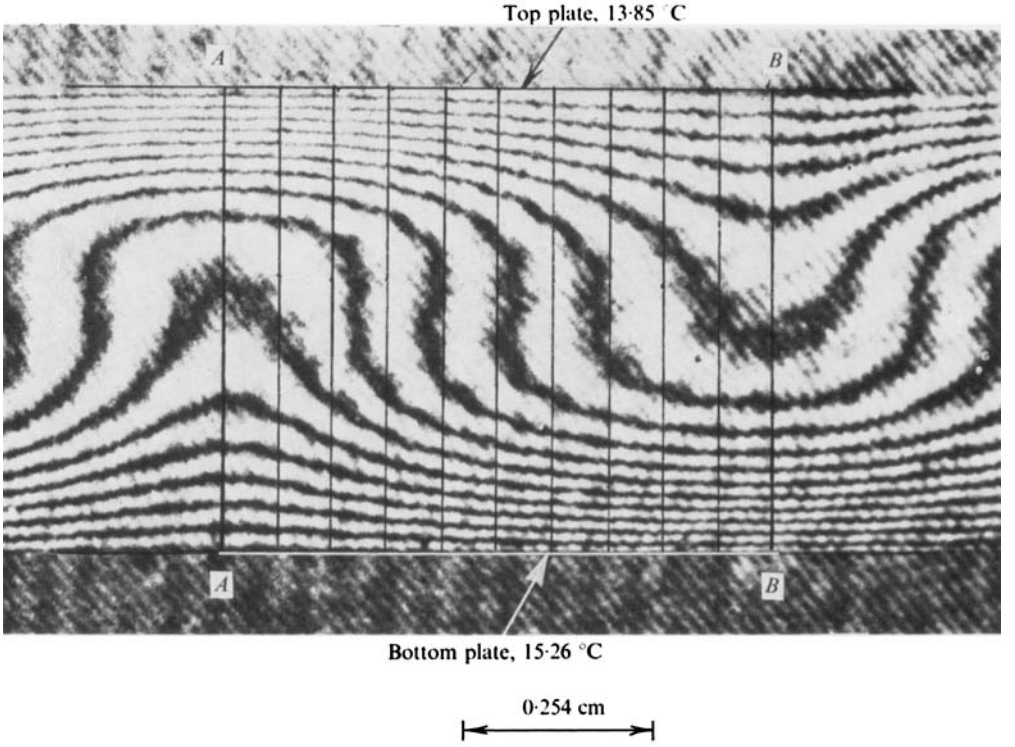


FIGURE 7. Enlarged portion of interferogram shown in figure 4(*c*). Vertical lines indicate positions where temperature profiles were measured. $Pr = 6{\cdot}8$, $R/R_c = 2{\cdot}8$.

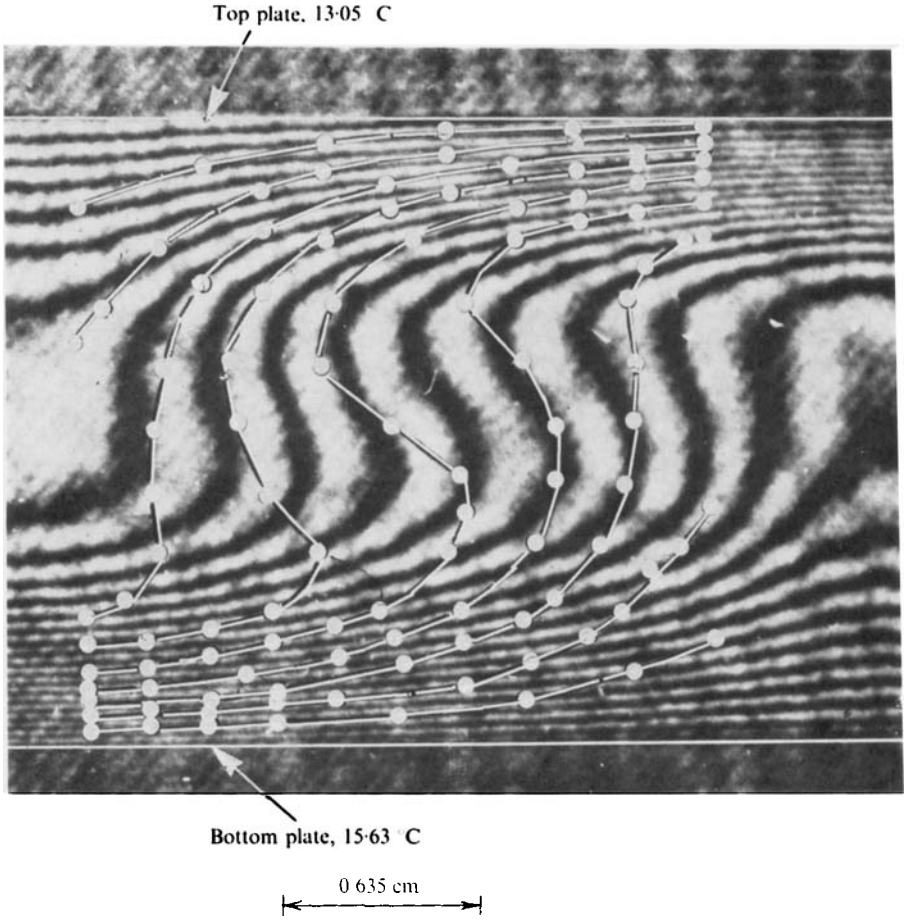


FIGURE 11. Interferogram for $R = 6460$ and $Pr = 6{\cdot}8$, with superimposed computed data points taken from Royal (1969), for which $R = 10000$ and $Pr = 0{\cdot}7$.